Title

Paleotsunami record of the past 4300 years in the complex coastal lake system of Lake Cucao, Chiloé Island, south central Chile

Authors

Philipp Kempf[1,2,*], Jasper Moernaut[3], Maarten Van Daele[2], Mario Pino[4], Roberto Urrutia[5], Marc De Batist[2]

*corresponding author: philipp.kempf@fu-berlin.de

Affiliations

1) Institute of Geological Sciences, Freie Universität Berlin, Berlin Germany
2) Renard Centre of Marine Geology, Ghent University, Gent, Belgium
3) Institute of Geology, University of Innsbruck, Innsbruck, Austria
4) Instituto de Ciencias de la Tierra, Universidad Austral de Chile, Valdivia, Chile
5) Centro EULA Chile, Universidad de Concepción, Concepción, Chile

Abstract

In CE 1960, Lake Cucao on Chiloé Island in south central Chile, was inundated by the tsunami of the Great Chilean Earthquake (M_w 9.5). The area of what is now the lake basin is submerged since the end of the rapid postglacial sea level rise and may have recorded tsunami inundations in its sedimentary record since then. Sub-bottom profiles and side scan sonar data reveal a tidal delta with a crosscutting channel, which controls the sedimentary environment in the coast-facing part of Lake Cucao. The convergent pattern of sub-bottom reflections near this channel indicates that tidal currents were active in the lake at least episodically since the formation of a major unconformity with strong reflection amplitude, i.e. the onset of lacustrine sedimentation. A radiocarbon date at the base of one of the 21 collected sediment cores dates this reflector to ~3800 yrs BP. Little net vertical displacement in combination with an outlet river channel that can act as a pathway for sediment transport appears to have maintained the sensitivity of Lake Cucao to record tsunamis in its sedimentary record. The sub-bottom profiles show a succession of antidunes, of which the geometry is used to reconstruct the flow speed and depth of the flow that formed them to 6.8 m s^{-1} and 4.8 m, respectively. The sedimentary record contains 15 clastic layers which are interpreted as tsunami deposits with a varying level of confidence. The confidence level on the tsunami interpretation depends on five criteria; there are site-specific criteria, i.e. i) high magnetic susceptibility of the sediment indicating high clastic content, ii) cross core correlation indicating widespread deposition, iii) acoustic reflector correlation to the sedimentary record (also indicating widespread deposition), and general criteria, e.g. iv) presence of mud clasts, and v) age correlation to known paleotsunamis in the area. In this way 8 clastic layers are interpreted as tsunami deposits with a high confidence level, 5 with a medium confidence level and 2 with a relatively low confidence level. The paleotsunami record of Lake Huelde, a mere 2 km north of Lake Cucao, contains 14 or 15 tsunami deposits in the same time interval, of which at least 10 can be correlated. This study adds a long paleotsunami record on a coastline where extreme tsunamis occur frequently and where long (>2000 yrs) paleotsunami records are still sparse. This study underlines the many challenges and extraordinary advantages

associated to paleotsunami research on coastal lakes and demonstrates how indispensable geophysical mapping and numerous coring sites can be in understanding the depositional environment of dynamic coastal lakes for extracting high-quality paleotsunami records.

Keywords

Tsunami deposits, lacustrine sediments, sub-bottom profiles, south central Chile, coastal sediment dynamics.

1 Introduction

Long and continuous sedimentary records of infrequent large-scale tsunamis are essential in characterising recurrence patterns – a requisite for reliable hazard assessments. During the past decades the scientific means to research the sedimentary record of tsunamis have grown in quantity and quality (Chagué-Goff et al., 2017, 2011). Linking tsunami deposits to tsunamis from documented history is a necessary step to calibrate tools in paleotsunami research. However, the primary reason for sedimentological investigations is to extend the historical record which is often not long enough to capture the variability in tsunami recurrence (Kempf et al., 2018). A challenging task, because long and continuous sedimentary records in often highly dynamic coastal areas are rare.

Written history in south central Chile begins with the Spanish invasion in CE 1541 (Cisternas et al., 2005; Lomnitz, 2004, 1970). In the ~500 years since then, four major earthquakes were chronicled in the area between the Arauco peninsula (~37°S) and the Chile Triple Junction (~46°S). The latest was the CE 1960 Great Chilean Earthquake (M_w 9.5), notorious for being the strongest earthquake on instrumental record. The older events occurred in CE 1575, 1737 and 1837. According to damage reports, tsunamis damaged coastal towns in all but the CE 1737 earthquake. Sedimentological investigations produced evidence for tsunami inundation for all three documented tsunamis in a multitude of coastal areas of Chile (Atwater et al., 2013; Cisternas et al., 2017, 2005; Dura et al., 2015; Ely et al., 2014; Garrett et al., 2015; Kempf et al., 2015; Nentwig et al., 2015; Reinhardt et al., 2010). In addition, six sites, i.e. Tirúa (Nentwig et al., 2018), Maullín (Cisternas et al., 2005), Caulle (Atwater et al., 2013), Chucalén (Garrett et al., 2015), Cocotué (Cisternas et al., 2017) and Lake Huelde (Kempf et al., 2017) are known to have recorded tsunami inundation before written history began (Fig. 1). Of these six sites, only the Maullín and Lake Huelde records extend the tsunami history past 1000 yrs BP, highlighting the need for adequate sites that have recorded a long sedimentary tsunami record.

One of the difficulties when researching tsunami deposits on millennial timescales, is relative sea level change, which plays a key role in tsunami deposition and preservation (Dura et al., 2016; Kelsey et al., 2015). Relative sea level rise creates the needed accommodation for tsunami deposit preservation in coastal lowlands. However, with too much relative sea level rise or fall or coastal erosion or progradation, the shoreline displacement may shift the area of tsunami deposition in respect to the previous tsunami deposit, which makes long and continuous paleotsunami records from coastal lowlands rare. In contrast, coastal lakes can provide excess accommodation and may be in a position with a stable sensitivity to record tsunami inundation since the culmination of the early Holocene sea level rise.

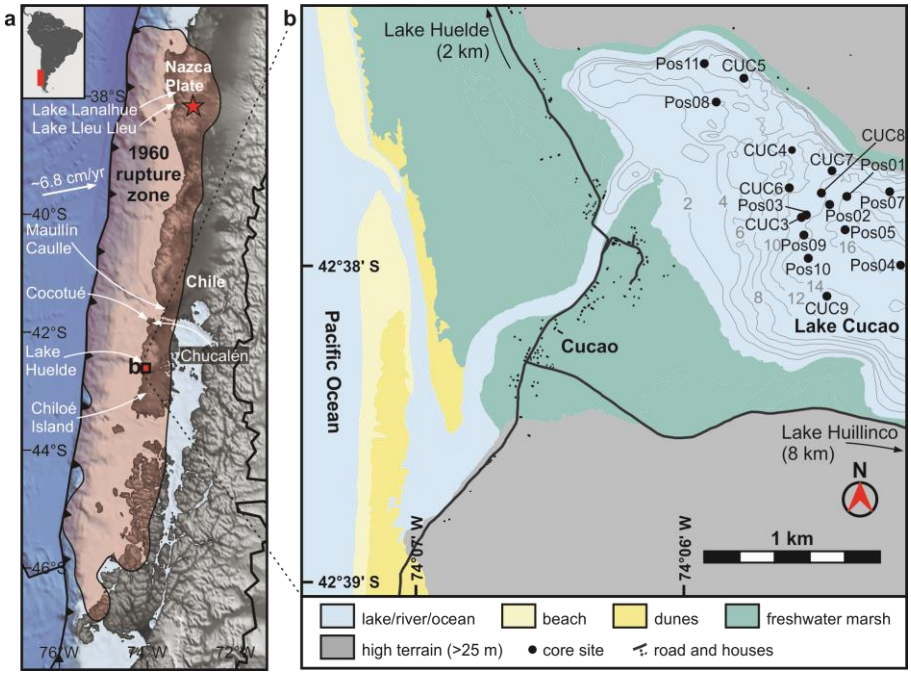

Figure 1: a) Topographic and bathymetric overview of south central Chile. The digital elevation model is based on the ETOPO1 dataset (Amante and Eakins, 2009). The epicentre and the 1 m slip contour line representing the rupture zone (Moreno et al., 2009) of the CE 1960 earthquake are drawn in red. Locations of coastal sediment records discussed in the text are indicated in white; b) detailed map of the study area. The geomorphological units are based on field observations and are extended using satellite imagery (Google Earth). The lake bathymetry map is based on side scan sonar bottom tracks (Kempf et al., 2015).

This study partially builds on a chapter in the doctoral thesis of the first author (Kempf, 2016). It presents a long and continuous sedimentary record from coastal Lake Cucao, with multiple tsunami deposits reaching back to ~4300 yrs BP based on a dense coverage of acoustic data and 21 sediment cores. The quality of the tsunami record is assessed by evaluating the sedimentary environment, tsunami deposit composition and age correlation with paleotsunamis in the region. The spatial multiproxy approach allows us to assign a confidence level to the interpretation as tsunami deposits, allowing a better evaluation of the temporal correlation of paleotsunamis.

2 Setting

Lake Cucao (74.09°W, 42.63°S) is a coastal lake located on the west coast of Chiloé Island in south central Chile (Fig. 1a). It is connected to the Pacific Ocean by its outlet river channel, which crosses the 1.3 km wide barrier of an up to 250 m wide beach, a narrow belt of active dunes followed by ancient dunes and pastures (Fig. 1b). Lake Cucao is an elongated lake with its long axis in NW-SE direction of 7.9 km and a width of ~1.5 km. It is 10.6 km^2 large and up to 25 m deep. It has a small catchment to lake surface ratio of 3.1:1, because of the upstream adjacent Lake Huillinco. The only direct riverine input is a small creek from the south in the eastern part. The outlet channel of the lake facilitates water exchange between lake and ocean in both directions, because the lake level lies in the intertidal zone (Kempf et al., 2015; Villalobos et al., 2003). The daily exchange of water forms a stable saline bottom water body in Lake Cucao and Lake Huillinco (Fig. 1) (Villalobos et al., 2003). With the transport of water from the Pacific

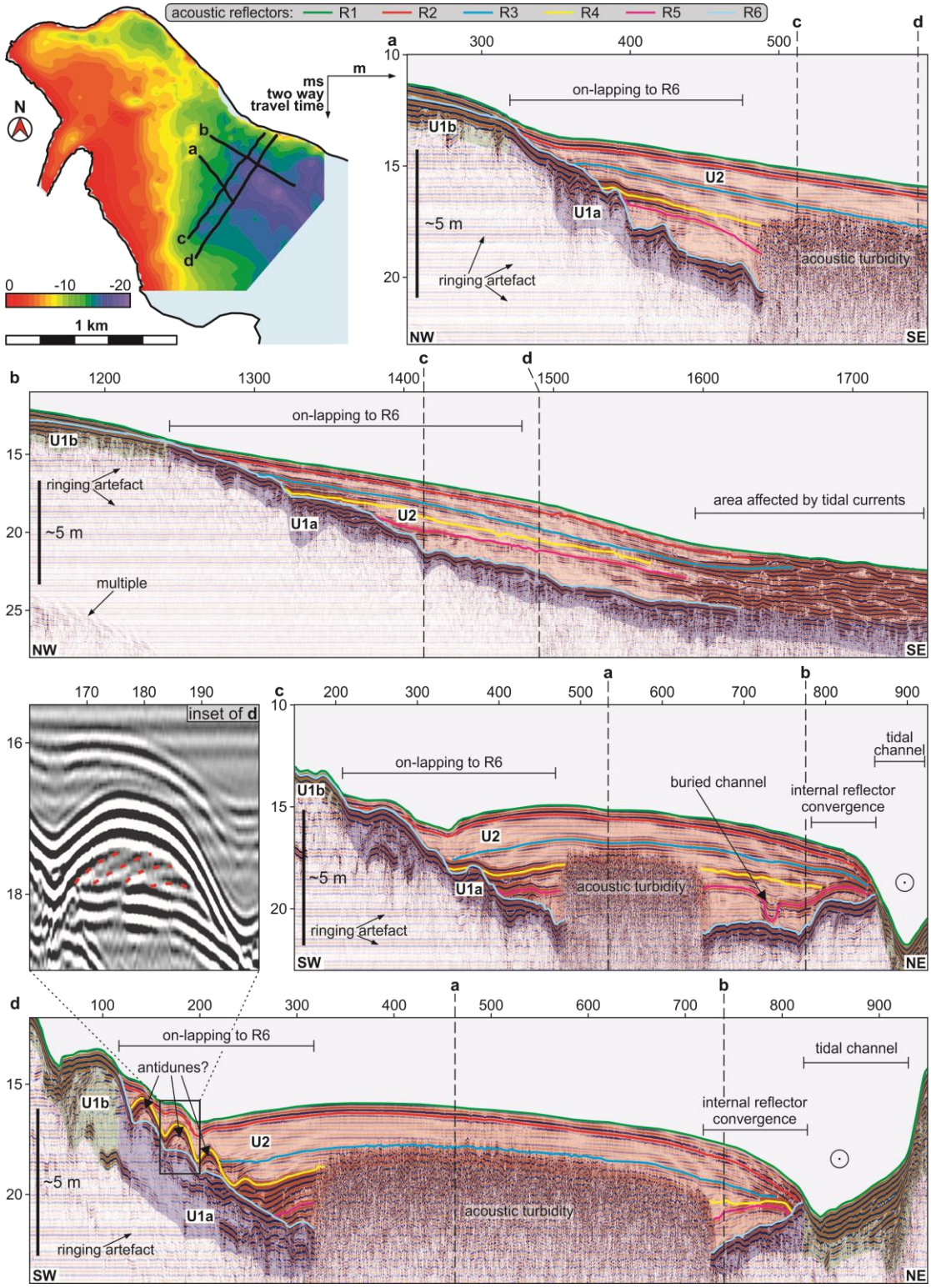

Figure 2: Sub-bottom profiles show the seismic stratigraphy of Lake Cucao with seismic units U1a (blue), U1b (green) and U2 (red). Profiles a) and b) parallel to the lake's long axis image the on-lapping of the internal acoustic reflectors R1–R5 onto acoustic reflector R6. Profiles in cross-direction to the lake's long axis c) and d) show down-lapping in the southeast and convergent internal reflectors towards the tidal channel. Reflector R4 expresses three hummocks (see inset), which are interpreted as antidunes.

comes erosion, transport and deposition of sediment, which produced a tidal delta around the outlet channel in Lake Cucao. Active mega-ripples on the tidal delta and a crosscutting channel through the delta are the bedform expressions of relatively strong present-day tidal currents (Fig. 2 and 3) (Kempf et al., 2015).

3 Methods

3.1 Acoustic imaging

The complex sedimentary system around Lake Cucao's outlet, was imaged with a Klein3000 side scan sonar, which uses 100 kHz and 500 kHz frequencies to produce a 50 m wide swath of the lake floor's acoustic reflectivity. The data was visualised with SonarWizMap v4 and has been presented in detail in Kempf et al. (2015). Here, we make use of the mapped mega-ripple crest outlines (Fig. 3).

We collected 25 km of high-resolution sub-bottom profiles with a 3.5 kHz GeoAcoustics GeoPulse pinger in 71 lines. At 3.5 kHz, the vertical resolution is between 10 and 20 cm. The data was visualised and interpreted with IHS Markit Kingdom v8.8. We use the sub-bottom profiles to

i) image the sedimentary architecture of the lake basin infill,
ii) to map geomorphologic features.
iii) to describe the general seismic stratigraphy,
iv) to determine coring sites,
v) to integrate the sediments cores with the acoustic data (ground truthing)

3.1 Sediment core analysis

In total, we cored at 21 locations in Lake Cucao, 9 of which were cored deeper than 2 m burial depth, with a maximum of ~8 m burial depth recovered. The top core section at each coring site is comprised of a gravity core, because gravity corers produce relatively undisturbed near-surface sediment samples. Any deeper core sections were obtained with a UWITEC hammer-driven piston corer. Deep and full recovery was achieved by overlapping 3-m-long core sections to produce composite cores. Both types of cores have a 6 cm inner diameter.

Each split core was analysed with a multi-sensor core logger (Geotek MSCL) for high-resolution line scan core surface imagery, gamma ray attenuation density logging and magnetic susceptibility logging (Bartington MS2E point sensor). The organic content was estimated using protocols in Heiri et al. (2001) for loss on ignition to 550 °C. Some core sections were X-ray CT-scanned with a Siemens Flash medical CT-scanner with a voxel size of ~0.15 × ~0.15 × 0.6 mm. Grain size distributions were measured with a Malvern Mastersizer 2000 after treatment with 2 ml of 35% hydrogen peroxide to dissolve organic content (where necessary this step was repeated), 1 ml of 10% nitric acid to dissolve calcareous content and 300 mg sodium hexametaphosphate to prevent grain flocculation. Material for radiocarbon dating was extracted by either identifying macrofossils or by wet-sieving 1 cm thick slices of sediment and picking remains of plants and periostraca in the sieve (Tab. 1).

The age control is based on 7 radiocarbon dates (Tab. 1) and the results of Kempf et al. (2015), who identified the youngest clastic layer as the CE 1960 tsunami deposit by the means of ^{137}Cs

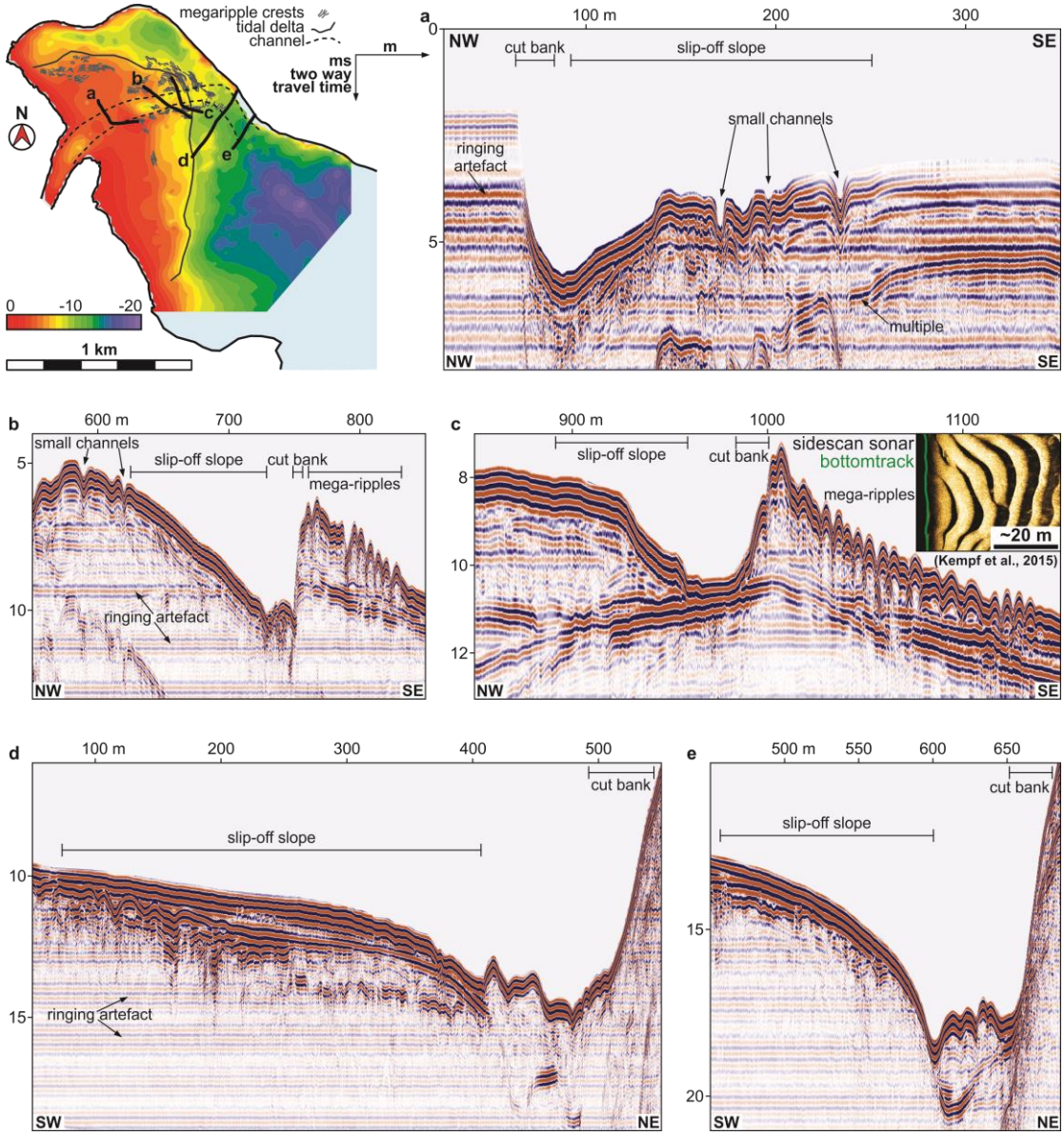

Figure 3: Sub-bottom profiles across the tidal channel expressing the asymmetry of the channel with alternating slip-off slopes and cut banks. Tidal currents produce mega-ripples outside the cut bank and small channels are present on the upper bank of the slip-off slope.

and ^{210}Pb-dating. The radiocarbon dates were calibrated using the southern hemisphere calibration curve SHCal13 (Hogg et al., 2013). The samples are comprised of leaves, small plant fragments and periostraca of (probably) *Diplodon chilensis* and fragments thereof. *Diplodon chilensis* is a freshwater species (Valdovinos and Pedreros, 2007).

4 Results

4.1 Seismic stratigraphy

Two seismostratigraphic units can be differentiated on sub-bottom data from Lake Cucao, U1 and U2 (Kempf et al., 2015). U1 (a and b) includes the acoustic base of the sedimentary infill. They laterally merge into one another. U1a is covered by the lake's sedimentary infill in relatively deep areas, whereas U1b is at least sporadically reworked by tidal currents entering

Table 1: Radiocarbon data for fossil leaves, plant fragments and periostraca from composite core Pos04, which is used as the master core for the age-control of the Lake Cucao sedimentary record.

sample ID	core ID	section depth	core depth in event-free age model	material	lab ID	14Cage	14Cage error
		cm	cm			14C yrs BP	yrs
CUCA10B-1.5	CUCA10B	1.5	142.5	shell fragment and plant fragments	UBA-37365	26178	161
CUCA10B-51	CUCA10B	51	190	plant fragments	UBA-37369	5189	56
CUCA11A-52	CUCA11A	52	246	plant fragments	UBA37370	2360	63
CUCA11A-101.5	CUCA11A	101.5	285.5	plant and periostracum fragments	UBA-37368	2166	34
CUCA11B-22	CUCA11B	22	313	plant fragments	UBA-37367	2342	33
CUCA11B-91.5	CUCA11B	91.5	353.5	periostracum	UBA-37364	2829	38
CUCA12B-82.5	CUCA12B	82.5	504	leaf	UBA-21476	3445	34

and exiting the lake in shallow areas near a tidal channel and not covered by lake infill (Fig. 2). U2 is the lacustrine sediment infill. The basal contact of U2 to U1a creates an unconformity (reflector R6) characterized by on-lapping reflector terminations towards the west. The internal reflector geometry of U2 in the upper part (above reflector R4) is parallel to sub-parallel with a low-amplitude acoustic facies including infrequent high amplitude, continuous reflections. (Fig. 2c). The lower part of U2 (below reflector R4) describes a more complex infill pattern with few internal unconformities.

The presence of shallow gas in the sediment of the central basin causes acoustic turbidity, which blanks the internal reflector geometry of U2 at depths greater than ~1.5 m (2 ms two-way-travel time, TWT). In total, five parallel to sub-parallel reflectors (R1–R5) can be traced within U2. R1 represents the lake floor and produces a continuous, strong reflection with decreasing amplitude towards the deeper lake basin in the southeast (Fig. 2). R2–R5 show high-amplitude, continuous internal reflections and form on-laps to either R6 or to one of the other internal reflectors, e.g. R4 on-laps to R5 in some areas. Of all internal reflectors, R4 has the highest reflection amplitude and marks the top of a hummocky paleo-surface in the south of the surveyed area (Fig. 2d). The hummocks are ~30 m long and ~1 m thick with up-slope dipping internal reflections. The two lowermost internal reflectors, R4 and R5, exhibit erosion of the underlying acoustically transparent lake sediment in the form of few buried channels (Fig. 2c).

The tidal channel incises the shallow delta up to 3.5 m deep and ~100 m wide, at its western end as a prolongation of the outlet river channel (Fig. 3a). The bathymetric cross-profiles of the channel are asymmetric with a flatter slip-off slope and a steeper cut bank of the channel (Fig. 3). The asymmetry alters along the channel. About 10 m wide and 0.5 m deep incised channels are common on the upper slip-off slope. Mega-ripples with about 8 m ripple wavelength and ~0.4 m ripple height are abundant around the incised channel, with a concentric arrangement (Kempf et al., 2015).The channel continues towards the north-eastern shore (Fig. 3b, c) and bends south-eastward to align with the long axis of the lake from where it continues parallel to the north-eastern shoreline (Fig. 3d, e). Towards the channel, the parallel to sub-parallel sedimentary infill of U2 (R1–R5) becomes convergent (Fig. 2c, d).

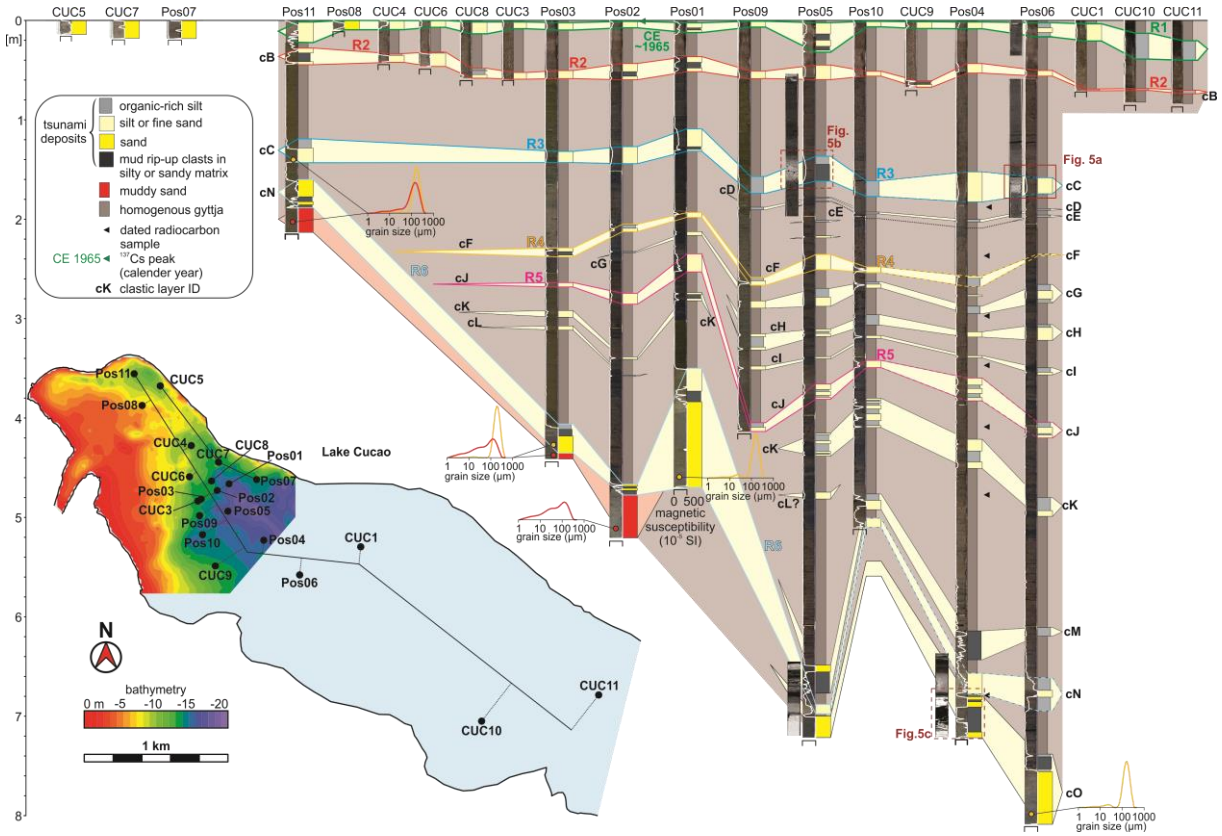

Figure 4: Core to core correlation of clastic layers in the organic-rich mud-dominated lake sediments. Cores are represented by a split core surface image, a sedimentological core log and in some cases 2D slices of CT-scans. The overview map shows two core transects through the lake. Cores CUC5, CUC7 and Pos07 are located in areas strongly affected by tidal currents. The white line on the split core surface images represents magnetic susceptibility. Grain size distributions are shown in 7 different positions to differentiate muddy sand of tidal delta foresets (red lines) from clastic layers (orange lines). Strong acoustic reflectors are drawn in the same colour as they are on sub-bottom profiles. The seismic to core correlation is captured in figure 6.

4.2 Lacustrine sedimentation

On the intertidal delta and in the crosscutting channel, i.e. areas where the top of U1b is at the lake floor, the sediment consists of a well-sorted medium to fine sand with mostly quartz, feldspar, hornblende and mica minerals (Fig. 4, e.g. core CUC7). The coarse and moderately to well sorted sand prevented penetration deeper than 20 cm with the coring equipment in these locations. This sand is mostly massive with some occurrences of 1 cm thick grey muddy layers. The magnetic susceptibility of this sand is very high, sometimes exceeding 1000 × 10^{-5} SI.

Sediment from the lake basin consists mostly of brown to black homogenous, poorly sorted organic-rich mud. The transition from black to brown mud can be gradual or sharp. In the case of sharp transitions, the brown mud is on top. The organic content for both black and brown mud is between 20 and 35 % and consists of seeds, fibrous plant material, pollen and fragments of bivalve periostraca without the calcareous shell. The periostraca are sometimes fully preserved with distinct growth rings and are probably from *Diplodon chilensis*, the most common

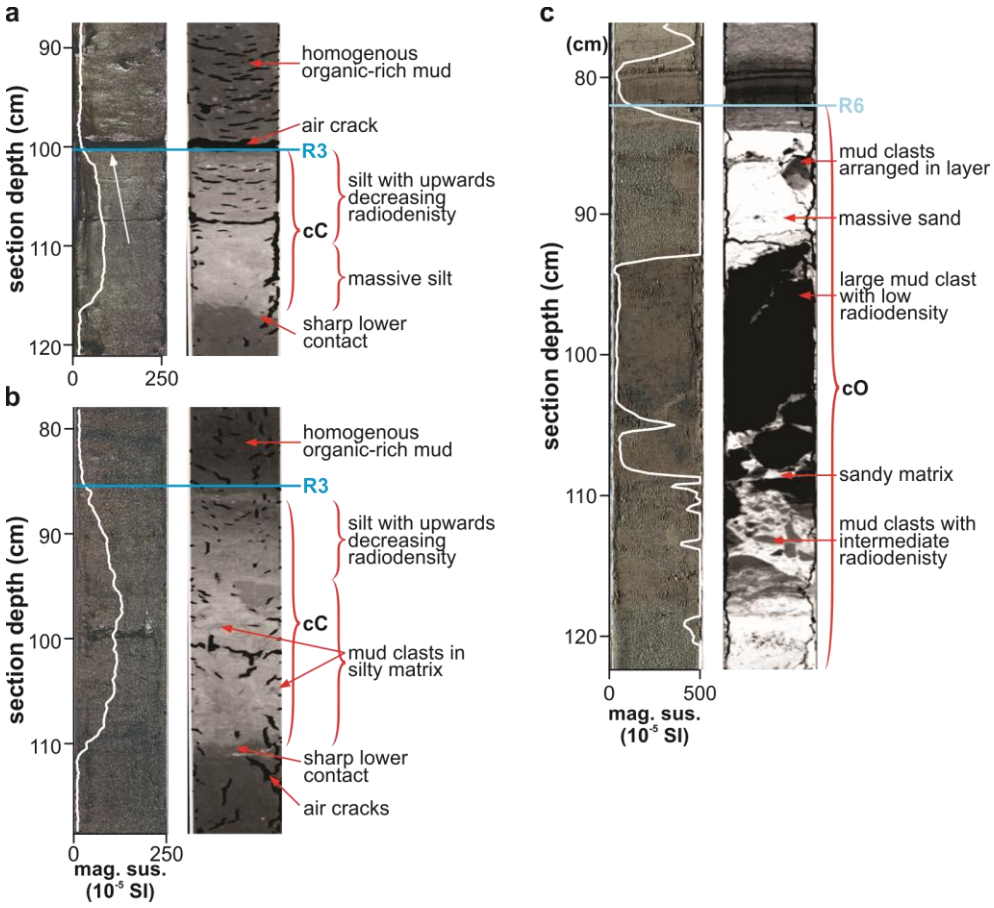

Figure 5: X-ray CT-scans of selected core sections. Lighter grey means higher radiodensity. a) and b) CT-scans of clastic layer cC associated acoustic reflector R3; c) clastic layer cN under acoustic reflector R6. All clastic layers exhibit a sharp contact at the bottom. CT-scans in a) and b) show upwards decreasing radiodensity. In b) and c) mud clasts with two differing CT-densities are surrounded by silty (b) to sandy (c) matrix.

freshwater clam in southern and south central Chile. The organic-rich mud smells strongly of hydrogen sulphide when cores are opened the first time (both during fieldwork and in the lab), indicating hypoxic or anoxic conditions. The magnetic susceptibility is low between 0 and 40 × 10^{-5} SI (Fig. 4 and 5).

In all 9 long cores, there are 1 to 30 cm thick layers with high clastic content. The medium silt to fine sand of the clastic layers is coarser than the clastic fraction of the organic-rich mud below and above. However, the clastic layers always contain a fraction of organic matter, too. The magnetic susceptibility signal of these layers ranges from relatively low, with values between 40 and 100 × 10^{-5} SI, to relatively high, with values up to 500 × 10^{-5} SI and higher (Fig. 4 and 5). The clastic layers are often visually indistinguishable from the organic-rich mud on the split core surface, except for black to brown colour contrasts. CT-scans of the clastic layers reveal sharp lower contacts with the highest radiodensity at the base, gradually decreasing upwards

(Fig. 5a, b). Some clastic layers bear 1 to 3 cm large mud clasts in a matrix of sand or silt. The mud clasts have lower radiodensity than the matrix and are discernible on CT-scan as darker bodies (Fig. 5b). The mud clasts were difficult to impossible to identify on split core surfaces

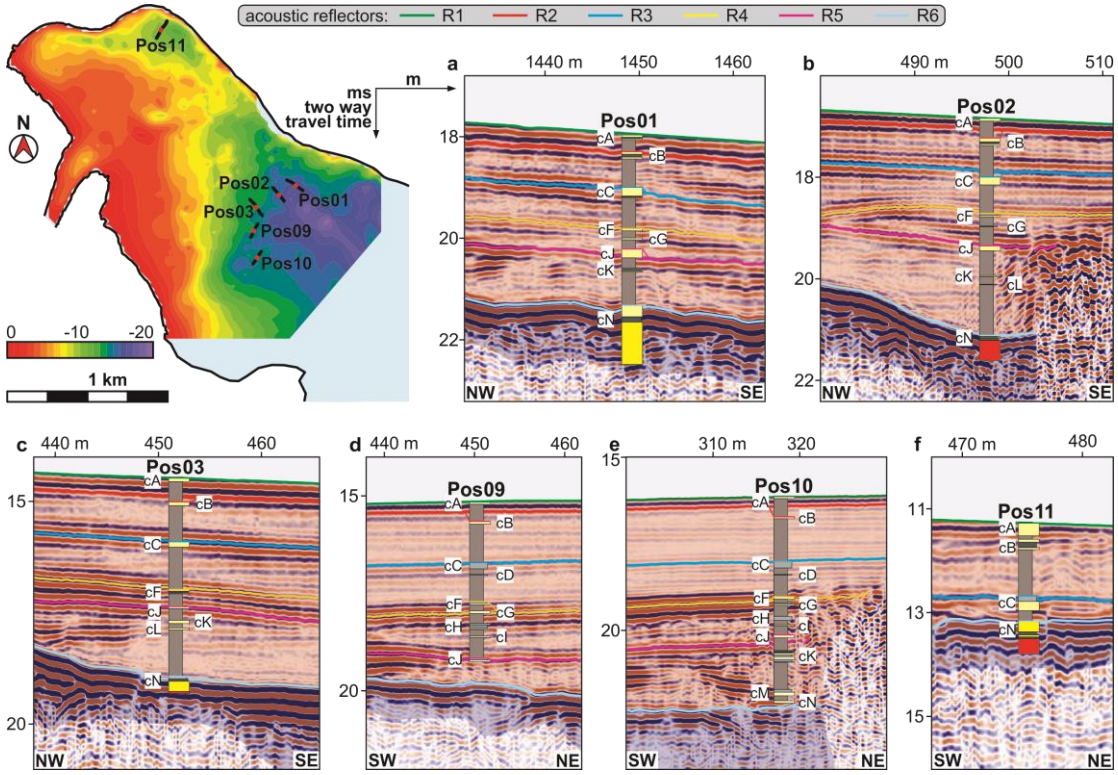

Figure 6: Seismic to core correlation of the CE 1960 tsunami deposit (cA) and clastic layers cB to cN (cO not represented on this figure) with strong acoustic reflectors R1 to R6. The assumption of uniform p-wave velocity within the entire lake infill and the piston coring process can cause minor offsets between cores and acoustic reflectors on sub-bottom profiles.

except for clastic layer cN. All other mud clasts were identified on X-ray CT-scans. If the clastic layers are brown, then they often coincide with a sharp colour transition from black to brown at their base. Some clastic layers have recognisable characteristics, e.g. thickness, colour, shape of the magnetic susceptibility log etc. that can be traced laterally throughout the basin. This way the easiest-to-trace clastic layers were correlated, helping with the correlation of the other clastic layers.

The clastic layers are labelled from cA to cO, where "c" stands for Lake Cucao and the capital letter is in alphabetical order down core. This is in analogy to the Lake Huelde record 2 km north of Lake Cucao, where similar layers interpreted as tsunami deposits, are labelled hC, hD, and so on to hQ (Kempf et al., 2017). The topmost clastic layer in Lake Cucao was identified in Kempf et al. (Kempf et al., 2015) as the tsunami deposit of the CE 1960 tsunami and will be called CE 1960, instead of cA.

Seven of 9 long cores contain the clastic layer cN in the lowest part of the sedimentary record, which is markedly coarser (fine to medium sand) and exhibits higher magnetic susceptibility values than the other clastic layers, with peaks up to 2500×10^{-5} SI. Like in all other clastic layers, the sand of cN does not contain mica. The lack of mica distinguishes the sand of the clastic layers from the sand in samples from the tidal delta and the crosscutting channel (Kempf et al., 2015). In cN, intervals of well-sorted massive sands are intercalated with intervals of mud clasts in a sandy matrix. The mud clasts can exceed the size of the core liner (6 cm) and are up to

Table 2: Summary of confidence levels for the interpretation of tsunami deposits for each clastic layer in Lake Cucao, with age and age-correlation to a known tsunami, maximum magnetic susceptibility, traceability of the clastic layers throughout the sedimentary record, correlation to acoustic reflections and content of mud rip-up clasts.

event name	median age (95% age interval)	potential age-correlation to published tsunami deposits	max. magnetic susceptibility	traceability in the sedimentary record	correlated to acoustic reflector	mud rip-up clasts	confidence level
	yrs BP		(10^-5 SI)	represented in cores/cores reaching this depth interval			
cA/CE 1960	-7 (-11 to -5)	yes	677	18/18	R1	yes	high
cB	287 (185 - 418)	yes	695	17/17	R2	yes	high
cC	1081 (894 - 1274)	maybe	1601	9/9	R3	yes	high
cD	1226 (1031 - 1418	yes	57	5/8	-	not observed	medium
cE	1274 (1079 - 1466)	maybe	51	2/8	-	not observed	low
cF	1656 (1454 - 1656)	yes	581	8/8	R4	yes	high
cG	1825 (1624 - 1986)	yes	431	7/8	-	not observed	medium
cH	1962 (1765 - 2109)	yes	202	5/8	-	not observed	medium
cI	2099 (1914 - 2213)	no	335	5/8	-	not observed	medium
cJ	2254 (2077 - 2322)	yes	306	8/8	R5	yes	high
cK	2530 (2378 - 2662)	yes	377	7/7	-	yes	high
cL	2883 (2670 - 3001)	no	92	3/7	-	not observed	low
cM	3699 (3530 - 3906)	yes	585	4/4	-	yes	high
cN	3783 (3612 - 3994)	yes	2269	8/8	R6	yes	high
cO (in model)	3798 (3626 - 4011)	no	1656	3/3	-	not observed	medium
cO (corrected)	4101 (3959 - 4344)	"	"	"	"	"	"

11 cm thick. Smaller mud clasts are often arranged along horizons (Fig. 5c). Based on the radiodensity of the mud clasts, two types can be differentiated; one type with a low radiodensity (black) and one type with an intermediate radiodensity (dark grey) (Fig. 5c). The sand of the matrix and intervals of massive sand contain grains of orthoclase, plagioclase, quartz, iron oxides (responsible for the high magnetic susceptibility), hornblende and rarely zircon, as well as lithic grains. The same composition of sand is reported for the CE 1960 deposit in Lake Cucao and Lake Huelde and for the beach sand and dunes sand between Lake Cucao and the Pacific Ocean (Kempf et al., 2015).

Three cores (Pos02, Pos03 and Pos11) contain poorly sorted, muddy sand at their base (Fig. 4). The muddy content makes this sand distinctly different in grain size from the well-sorted sand in the coarser clastic layers, e.g. clastic layers cC and cN. It consists of the same minerals and lithic grains as the sand on the tidal delta and in the channel.

4.3 Sub-bottom profiles to core correlation

Six of the long cores were projected on sub-bottom profiles that show acoustic penetration of the entire seismic unit U2 (Fig. 6). The correlation between cores and the sub-bottom profiles is performed under the assumption of a constant p-wave velocity in the entire sedimentary sequence and no vertical deformation during hammer-driven piston coring and then tying key marker layer with the sub-bottom profile. Realistically, variability in p-wave velocity is expected to produce minor offsets. The vertical deformation during hammer coring will cause net compression and wave action on the lake while coring can cause extension, which will likely be heterogenous and may produce significantly larger offsets. Some offsets are indicated on the sub-bottom profiles to core correlation (Fig. 6).

The six reflectors of U2 (R1 to R6) can all be confidently correlated to clastic layers in the cores (Fig. 4). The top of the CE 1960 tsunami deposit is buried by ≤ 3 cm of lacustrine sediment in the western part of Lake Cucao (Kempf et al., 2015), which is below the vertical resolution of the sub-bottom profiles (vertical resolution between 10 and 20 cm). R1, the uppermost strong reflector therefore correlates to the lake floor as well as the top of the CE 1960 tsunami deposit. R2 correlates to clastic layer cB. However, R2 is so close to the lake floor and R1 reflection, that interference of reflections may lead to a poor identification of R2 in most cases. R3 correlates to cC, R4 to cF and R5 to cJ, which are major traceable clastic layers in the sedimentary record of Lake Cucao. They tend to be especially thick and coarse, and are represented in most or all cores containing that specific stratigraphic interval. R6 is the reflector that sticks out, because reflectors R2 to R5 on-lap to it. Even though a spatial feature such as on-lapping is difficult to observe by comparison of multiple cores, clastic layers cF to cM appear to on-lap to cN (Fig. 4). Because of its stratigraphic position, the on-lapping and the strong sedimentary contrast between organic-rich mud and the medium sand of clastic layer cN, we correlate the high-amplitude reflector R6 to the coarse clastic layer cN (Tab. 2).

4.4 Age control

The clastic layers exhibit characteristics of abrupt deposition, e.g. sharp lower contacts, mud clasts and decreasing upwards radiodensity, which often reflects fining upwards (cf. Van Daele et al., 2014). The intervals of the clastic layers are therefore likely to have been deposited with a different accumulation rate from the rest of the sedimentary record, most likely quasi-instantaneously.

We used composite core Pos04 to develop an age-depth model for Lake Cucao. The prior age-depth information consists of the following data and considerations:

i) radionuclide data that identified the CE 1960 tsunami deposit (Kempf et al., 2015)
ii) 7 radiocarbon dates (Tab. 1)
iii) clastic layers were treated as instantaneous deposits, i.e. they were taken out of the core for age-depth modelling
iv) the sediment is a lacustrine sedimentary sequence, so we assume a relatively stable sedimentation. This is supported by the uniform nature of the sediment sequence with parallel reflections on sub-bottom profiles at the core site.

All age-depth information of Pos04 was fed into the autoregressive Bayesian age-depth modelling algorithm BACON (Blaauw and Christen, 2011). The parameters were adjusted to divide the core into 178 sections of 3 cm and to reflect the relatively stable lake environment, i.e. continuous sedimentation of the organic-rich lacustrine mud (Fig.7).

The model output shows that there are two obvious outliers, i.e. extreme age reversals, among the radiocarbon dates (samples CUCA10B-1.5 and CUCA10B-51), which were neglected by the age-depth algorithm for making the age-depth model. From the resulting age-depth model we extracted the age probability distributions of all clastic layers that were treated as instantaneous deposits (Fig. 7). The problem connected to the relatively long interval of interpolation between the core top and the shallowest radiocarbon date (2360 ± 63 yrs BP) is minimised by the relatively stable sedimentary environment at core site Pos04.

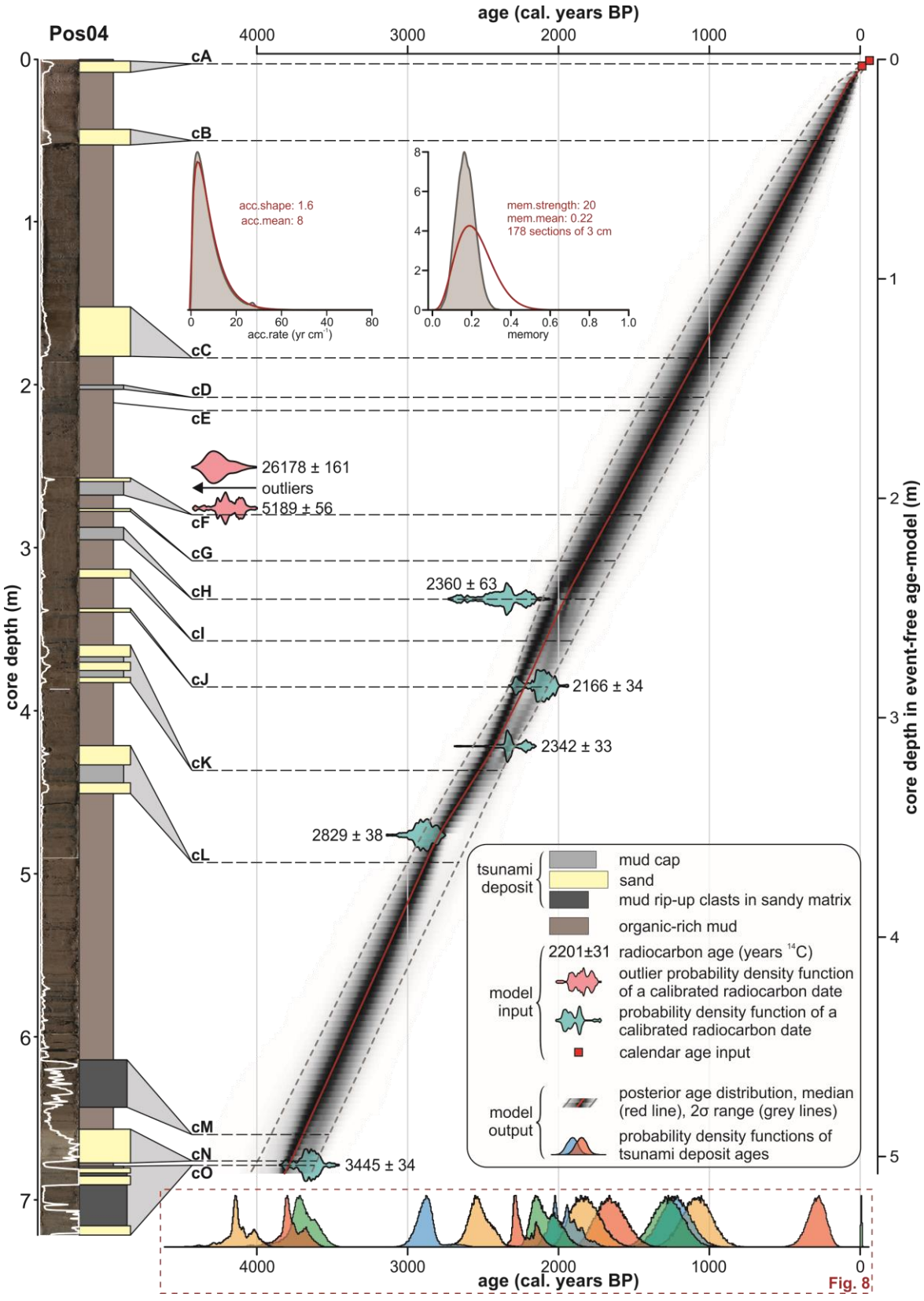

Figure 7: Bayesian age-depth model of core Pos04 in Lake Cucao calculated with BACON (Blaauw and Christen, 2011). The core surface image and sedimentological core log are displayed on the left. The tsunami deposits are treated as instantaneous deposits and are taken out of the core for age-depth modelling. The bottom x-axis shows the model results for all tsunami deposits as coloured age distributions.

The assumption of relatively stable accumulation rates in Pos04 (iv) appears to fail only at the lowest end of the sedimentary record (between clastic layers cN and cO). This becomes evident when comparing the 2 cm thick organic-rich mud interval in core Pos04 with the 43.5 cm thick organic-rich mud interval of the same stratigraphic position in core Pos06. The age-depth model on core Pos04 likely underestimates the time difference between clastic layers cN and cO. Using the average accumulation rate of the entire record down to clastic layer cN of ~1.31 mm yr^{-1} (502 cm of sediment accumulation in 3845 years), clastic layer cO is probably ~330 years older than clastic layer cN.

5 Discussion

5.1 Antidunes as a product of tsunami inundation in Lake Cucao

The hummocks with the up-slope dipping internal reflectors underneath R4 (clastic layer cF) are interpreted as antidunes due to their height and length in combination with the up-slope dipping internal reflectors. Antidunes form in the upper stage supercritical flow regime. The wavelength of antidunes is related to the wavelength of the standing wave that produced them (Allen, 1984), which in turn is proportional to the square of the flow speed during formation (Kennedy, 1963). The resulting relationship between flow speed and wavelength of the antidune bedform is described by Carling (2009) with

$$U = \sqrt{\frac{g\,L_a}{2\pi}} \qquad (1)$$

Where U is the flow speed, g the gravitational acceleration on earth and L_a the average wavelength in a train of antidune bedforms. The flow depth d in dependence on average wavelength is expressed by

$$d = \frac{L_a}{2\pi} \qquad (2)$$

According to equation (1) the flow speed during antidune formation was ~6.8 m s^{-1} (24.6 km h^{-1}) and according to equation (2) the flow depth was ~4.8 m. Both dimensions compare well with directly measured flow properties of recent large-scale tsunami inundations (cf. Fritz et al., 2012). The location of the antidunes suggests that the freshwater marsh, which now accommodates most inhabitants of the village of Cucao was washed over by strong, certainly destructive water currents. Despite their size, antidunes form relatively quickly once supercritical flow develops. However, with three antidunes of similar shape and size, we argue that supercritical flow was well developed, steady and sustained.

5.2 Age control and accumulation rate variability in Lake Cucao

There is no overall strong spatial variability in accumulation rate between long cores from the western part of the basin, which is indicated by sub-parallel clastic layers in the core to core correlation. This is confirmed by parallel to sub-parallel reflectors R1 to R5 on sub-bottom profiles (Fig. 2a, b).

There are three exceptions, which are

i) confined areas of erosional truncation in form of small channels (Fig. 2c),

ii) the area close to the crosscutting channel along the north-eastern side of the lake, where the sedimentary infill becomes significantly thinner or is non-existent (Fig. 2c, d), and

iii) the deepest part of most long cores, where the strata form on-laps (this includes the age-depth modelled core Pos04 between cN and cO).

All long core sites avoid the areas of i) and ii).

In short cores CUC10 and CUC11, located 2–3 km southeast of most other cores (Fig. 4), and where tidal currents are probably weaker or absent, up to 21 cm of organic-rich mud accumulated above the CE 1960 tsunami deposit. This thickness is comparable to 20–30 cm of post-1960 sediment accumulation in Lake Huelde (Kempf et al., 2015), which is currently unaffected by tidal currents. In all other cores further west in Lake Cucao the same interval is either ≤ 4 cm thick or missing, showing non-deposition or episodes of erosion in the post-1960 lake environment in the ocean-proximal area of the lake.

The age-control of the last 2000 yrs relies strongly on the assumption of stable accumulation rates between the CE 1960 tsunami deposit and the uppermost useful radiocarbon date at 246 cm (event-free core depth) (Fig. 7, Tab. 1). Cores and sub-bottom profiles justify this interpolation, because of the uniform stratigraphy with little lateral variability in this part of the stratigraphic record of U2 near the coring site Pos04.

Chronologies of other regional paleotsunami and paleoseismic records from south central Chile are based on similar primary age-depth information, i.e. on radiocarbon dates of plants flattened by the tsunami, rootlets in soil, terrestrial plant fragments from the pre- and post-tsunami lacustrine sediment and tephras (Atwater et al., 2013; Cisternas et al., 2017, 2005; Garrett et al., 2015; Kempf et al., 2017; Moernaut et al., 2018, 2014). The uncertainty intervals of tsunami ages in the Lake Cucao record are greater than the uncertainty intervals of the tsunami ages of, for example, the paleotsunami record of Lake Huelde. Nevertheless, the Lake Cucao ages correlate well with regional paleotsunami records (Fig. 8). The age-control can be considered of comparable quality.

5.3 Age of the crosscutting channel and constraints on Lake Cucao's vertical displacement history

Coastal areas on subduction zones are known to be prone to vertical deformation throughout the seismic cycle (Wesson et al., 2015). The CE 1960 Great Chilean Earthquake caused the area around Lake Cucao to subside co-seismically by ~1 m (Plafker and Savage, 1970), which put Lake Cucao into an intertidal position, if the lake level was not already in the intertidal zone before. The subsidence of ~1 m may have intensified the tidal currents, which would explain the limited post-CE 1960 sedimentation in all but the most distal coring sites. The tidal currents entering the lake during high tide are continuing to form the intertidal delta, the crosscutting channel and the mega-ripples. Given that the sedimentary record below the CE 1960 tsunami deposit appears to have stable accumulation rates, we argue that the vertical position of the river channel in relation to the relative sea level is probably at an extreme low at present in respect to the last 4300 yrs.

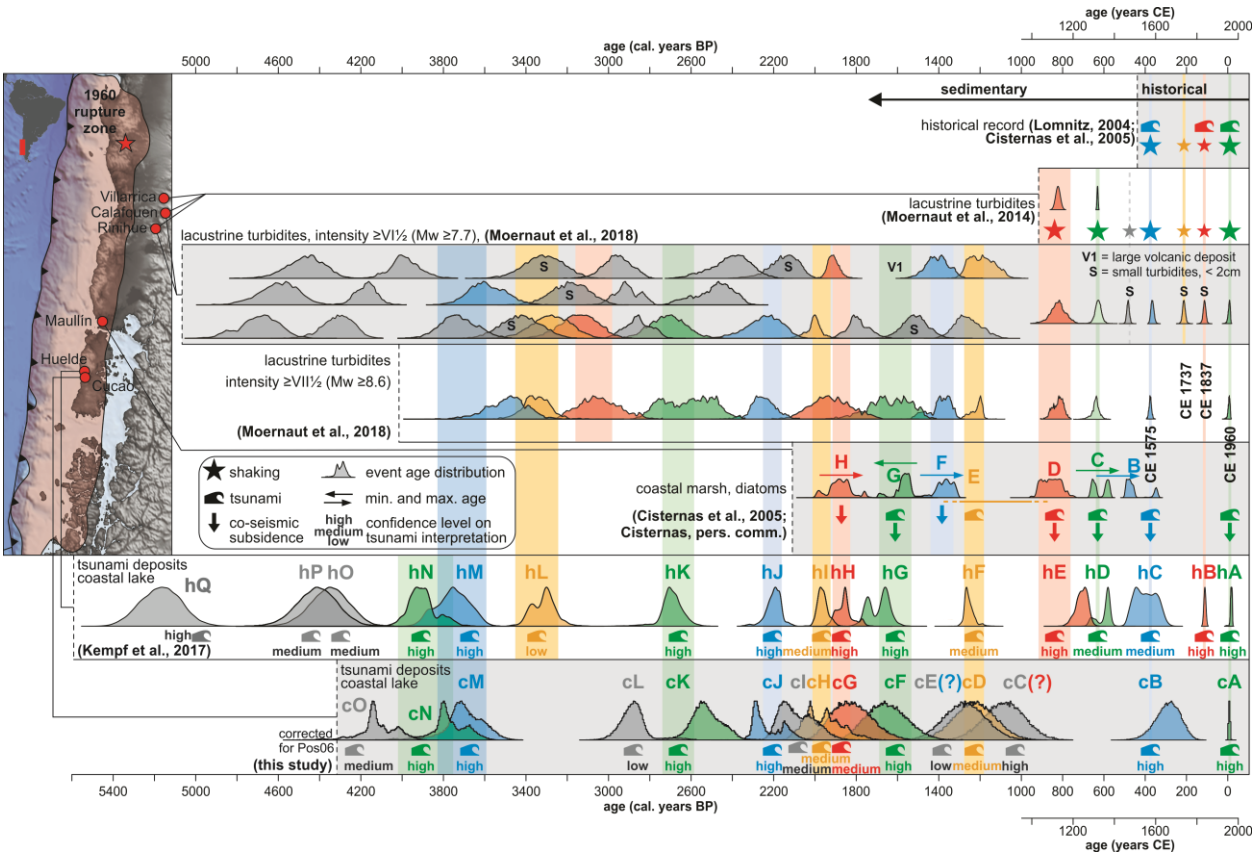

Figure 8: Regional correlation of paleoseismic and paleotsunami records. The instrumental record only includes the CE 1960 event and is not especially listed here. Documented history reveals three more large events in CE1575, 1737, 1837 (Cisternas et al., 2005; Lomnitz, 2004). Lacustrine turbidites from the Chilean lake district give paleoseismic evidence (Moernaut et al., 2018, 2014). The paleotsunami records from Maullín (Cisternas et al., 2005) and Lake Huelde (Kempf et al., 2017) offer the direct comparisons between tsunami deposits. The age of cO is here corrected by 330 yrs because of the regular organic-rich lacustrine sediment between cN and cO in core Pos06 (in contrast to core Pos04 for which the age-depth model was made).

If the channel would be a recently formed feature, it would truncate the mostly parallel to sub-parallel internal reflectors of seismic unit U2. This is not the case; all internal reflectors, R1 to R5, in U2 converge towards the channel (Fig. 2c), which indicates that intertidal currents were active at least episodically during the period represented by the sedimentary infill visible on sub-bottom profiles. This constrains the net vertical displacement of Lake Cucao in the last 4300 yrs to a narrow window around its current position.

Additionally, river channels play a primary role in connecting the ocean with coastal lakes during tsunami inundation (Kempf et al., 2017, 2015). Consequently, regardless of the exact position of the coastline and river channel migrations, Lake Cucao may have been a reliable tsunami recorder with relatively stable sensitivity to tsunami inundation in the past 4300 yrs and potentially longer.

5.4 Identifying tsunami deposits in the Lake Cucao sedimentary record

The clastic layers share similar sedimentary characteristics to the tsunami deposit of CE 1960. However, other causative processes must be excluded before a tsunami origin can be assigned.

Tsunami deposits have several sedimentary characteristics, most are site-specific, and few are unique to tsunami deposits. For example, landwards thinning and landward fining sand sheets can be produced by storm surges and tsunamis alike (Kortekaas and Dawson, 2007). However, the relatively distant inland location (~1.3 km between ocean and lake) makes storm deposition in Lake Cucao unlikely. While storms occur on the south central Chilean coast, the tropical cyclones with the potential to create deposits kilometres inland and in coastal lakes, have not been documented and are unlikely to happen, even under strong El Niño conditions (Fedorov et al., 2010).

Excluding competing hypotheses for the formation of similar layers is equally valuable. For Lake Cucao we can, for example, exclude flood turbidites, which are not uncommon in Chilean lakes (e.g. Van Daele et al., 2019), because upstream adjacent Lake Huillinco traps riverine flood input to Lake Cucao, which reduces the direct riverine input to Lake Cucao to a small creek that enters Lake Cucao from the south in its eastern part. The small creek does not have a large enough catchment to produce lake-wide flood turbidites. And if it were to produce flood turbidites the fining of sediment would be away from the inflow of the creek, i.e. east to west in the study area and not west to east.

We define the following five criteria for the sedimentary environment of Lake Cucao, which are either indicative of tsunami deposition or can be used to exclude other processes.

i) *High magnetic susceptibility* – Magnetic susceptibility is controlled by the ferrimagnetic mineral content of the sediment. High magnetic susceptibility in Lake Cucao means the sediment contains iron oxides (i.e. hematite and magnetite). The concentrations of ferrimagnetic minerals in the basin of Lake Cucao can be increased by organic matter depletion, compaction or by deposition of iron oxides. The low magnetic susceptibility values of organic-rich mud and the sometimes extremely high values of magnetic susceptibility in the clastic layers suggest that the layers with high magnetic susceptibility values are from extra-lacustrine sources. Processes that could provide such a sediment source are limited to lake-inundating events, such as storms and tsunamis. This effect has been described for the CE 1960 tsunami deposit (Kempf et al., 2015).
ii) *Traceability in the sedimentary record* – Tsunami deposits in coastal lakes are spatially variable in thickness (Kelsey et al., 2005; Kempf et al., 2017). However, tsunami deposits are often continuous deposits to where they wedge out towards their maximum lateral extent. When tsunamis inundate coastal lakes, the water flow contains and deposits sand, remobilises muddy lake sediment and redistributes it within the lake basin. Areas beyond the zone of sandy deposition can receive exclusively muddy tsunami sediment (Kelsey et al., 2005; Kempf et al., 2017, 2015). Therefore, tsunami deposits should be traceable in the sedimentary record throughout large areas of the lake, if not the entire lake basin. The criterion is given as a fraction of the number of cores, in which the clastic layer is observed over the number of cores, in which the stratigraphic interval of the clastic layer in question was recovered. Complete or nearly complete representation in the sedimentary archive is treated as indicative for tsunami deposition (Fig. 4).
iii) *Acoustic reflector correlation* – The six strong reflectors (R1–R6) on the sub-bottom profiles represent strong contrasts in acoustic impedance, i.e. differences in p-wave velocity and/or density. In an organic-rich mud-dominated environment high acoustic

impedance contrast can be associated with clastic layers. Not every clastic layer will necessarily produce a high-amplitude reflector, but if a clastic layer can be correlated to a basin-wide high-amplitude acoustic reflector, then this points towards basin wide distribution and high clastic content, which is expected from a tsunami deposit.

iv) *Mud rip-up clasts* – We interpret the mud clasts as mud rip-up clasts. Mud rip-up clasts are generated by high-energy processes in otherwise low-energy environments. In sub-aquatic landslides, mud rip-up clasts occur on the spectrum of disintegration of the sliding sediment from slumps, to debris flows, to turbidity currents (cf. Lee et al., 2013). Onshore landslides that impact muddy fjord sediment have also produced mud rip-up clasts, which may show paleo flow direction by imbrication (Van Daele et al., 2014). In fluvial systems mud rip-up clasts are associated with cut bank collapses of muddy soils. In coastal environments, like marshes, mud rip-up clasts are commonly associated with tsunami deposition (Peters et al., 2007), however, storm surges reportedly can produce mud rip-up clasts, too (Phantuwongraj et al., 2013). In Lake Cucao, two types of mud rip-up clasts can be differentiated by their radiodensity. One type has the same radiodensity as the lacustrine organic-rich mud and is interpreted as such. The other type has higher radiodensity and could represent soil from the lake-surrounding marshes. Similar variations in mud rip-up clasts were described in trenches on the Chilean main land near Maullín (Atwater et al., 2013). Specifically for Lake Cucao, the presence of both types of mud rip-up clasts excludes strong tidal currents and slope failure turbidites. Tidal currents could work similarly to fluvial systems with regard to the erosional process for the source material of mud rip-up clasts and to the depositional process of clastic layers.

v) *Age-correlation* – Megathrust earthquake-induced tsunamis hit long stretches of coastline. Tsunami deposits can be correlated over long distances using their chronology (Cisternas et al., 2017; Peters et al., 2007). If a clastic layer correlates in age to an identified tsunami deposit elsewhere in south central Chile, then this corroborates the interpretation as a tsunami deposit. In the Lake Cucao sedimentary record, the interpretation of the CE 1960 tsunami deposit was partially based on such an age correlation. Downcore, age-correlation with the Lake Huelde sedimentary record (Kempf et al., 2017) is especially interesting, because of the lakes' proximity (2 km) to each other and the similarity of the paleotsunami record, despite the difference in lacustrine sedimentary environments.

Two of the 15 clastic layers (cE, and cL) fulfil only one or no criterion at all. The confidence of an interpretation as a tsunami deposit in these cases is low, however, a tsunami origin is probably still the most favourable hypothesis (Tab. 2). Eight clastic layers fulfil three or more criteria and the confidence level for interpreting these layers as tsunami deposits is high. The remaining 5 clastic layers fulfil two criteria sufficiently and receive a medium confidence level.

The Lake Cucao record potentially matches with 10 regionally known paleotsunami and paleoseismic events (Fig. 8, Tab. 3). Additionally, deposit cC matches to some extent with deposit hE in Lake Huelde and event D in Maullín, but weaker age control in the Lake Cucao record for the last ~2000 yrs may inhibit a conclusive correlation. The confidence level for both event deposit hE and cC are high, which supports the hypothesis of same origin, because in no other instance is there a high confidence tsunami deposit in Lake Huelde without a matching

Table 3: Regional age-correlation of paleotsunami and paleoseismic events.

historical record	Cucao	Huelde	Maullín	Rinihue Calafquen Villarrica
year of event	name in record (confidence level)	name in record (confidence level)	name in record	correlating event
1960	**cA (high)**	**hA (high)**	**A**	**yes**
1837	-	hB (high)	-	yes
1737	-	-	-	yes
1575	**cB (high)**	**hC (medium)**	**B**	**yes**
beyond record	-	hD (medium)	C	yes
	cC (high) (?)	hE (high)	D	yes
	cD (medium)	**hF (medium)**	**E**	**yes**
	cE (low) (?)	-	F	(?)
	cF (high)	**hG (high)**	**G**	**yes**
	cG (medium)	**hH (high)**	**H**	**yes**
	cH (medium)	**hI (medium)**	beyond record	**yes**
	cI (medium)	-		(?)
	cJ (high)	**hJ (high)**		**yes**
	cK (high)	**hK (high)**		**yes**
	cL (low)	-		no
	-	hL (low)		yes
	cM (high)	**hM (high)**		**yes**
	cN (high)	**hN (high)**		(?)
	cO (medium)	-		(?)
	beyond record	hO (medium)		(?)
		hP (medium)		(?)
		hQ (high)		beyond record

tsunami deposit in Lake Cucao and vice versa. The only exception is the cryptic CE 1837 tsunami deposit, that was recognised in Lake Huelde by IRSL dating (Kempf et al., 2015).

Deposit cE matches well with event F in Maullín, however, Lake Huelde does not record tsunami deposition in this period and in Maullín the event was only recognised by co-seismic subsidence and not with a tsunami deposit (Tab. 3) (Cisternas et al., 2005; Kempf et al., 2017). Either Lake Cucao was relatively sensitive to tsunami inundation at the time and recorded a minor tsunami that had no sedimentary impact in Maullín, Lake Huelde and other regional paleotsunami records. Or as the low confidence level denotes, deposit cE is potentially not a tsunami deposit.

Both deposits cL and hL have only a minor sedimentary imprint in Lake Cucao and Lake Huelde, respectively, with low confidence level on the interpretation as tsunami deposits (cf. Kempf et al., 2017). If either deposit is a tsunami deposit, then the origin

is probably a minor tsunami. The age-depth modelling in both records does not match the two deposits, so that it can be concluded that they are most likely not from the same event.

In contrast, for example, deposits cK and hK from Lake Cucao and Lake Huelde, respectively, share a similar clear (high confidence level), but not extreme sedimentary imprint in their

548 respective records. The age-depth models match the two deposits, so it is likely that cK and hK
549 were deposited during the same tsunami inundation event.

550 ***5.5 Spatial perspective on tsunami deposits in a lake basin***

551 Event maps (Figs. 9 and 10) that summarise the sedimentary characteristics of the tsunami
552 deposits visualise spatial trends of the tsunami deposits. The following conclusions are supported
553 by the spatial data.

554 i) Mud rip-up clasts are limited to the proximal part of the lake basin (Fig. 9). The
555 tsunami deposit cO at core site Pos04 is the only exception. This trend seems
556 plausible as it requires high energy water flow to erode and transport mud rip-up
557 clasts. Dissipating energy in the fluid flow over distance would dictate that mud rip-
558 up clasts would be the first particles to resist transport or remobilisation.
559 ii) For a large extent in the lake basin, tsunami deposits do not decrease in thickness.
560 This contradicts the spatial trend in onshore tsunami deposits, where tsunami deposit
561 thickness is influenced by the onshore morphology and tends to decrease with
562 increasing run-up distance (Goto et al., 2014). This study has thickness data along up
563 to ~3 km of inundation distance. Even for the tsunami deposit thickness data from CE
564 1960 and CE 1575 (cB) with a ~3 km long transect no decreasing trend in thickness
565 can be recognised. Logically, in the most distal parts of the record the tsunami deposit
566 must wedge out, however, the core sites are not located in the area where this occurs.
567 iii) From the location where a tsunami deposit has a muddy component, the muddy
568 characteristic in the tsunami deposits is always present in more distal locations.
569 Examples are the tsunami deposits cF, cK or cM. This highlights one aspect of the
570 reliability of coastal lakes to record tsunami deposits.
571 iv) To record tsunami deposition over large parts of a lacustrine basin, muddy grainsizes
572 can be sufficient, e.g. tsunami deposit cD (Fig. 9). However, detection of those
573 deposits is more difficult, because of the similarities to the surrounding regular
574 lacustrine sediment. In the case of the muddy tsunami deposits in Lake Cucao the
575 magnetic susceptibility was enough to indicate candidate clastic layers. In
576 environments, where magnetic susceptibility cannot be used, other methods need to
577 be tested, e.g. XRF scanning or a bio-marker analysis.

578 ***5.6 A conceptual model towards the origin and evolution of the lake basin***

579 In order to contrive a conceptual stratigraphic model of Lake Cucao that incorporates all
580 sedimentologic evidence available, we begin with the topographical depression that is now
581 occupied by Lake Cucao. The depression was a glacifluvial river valley (Glasser et al., 2008),
582 which was submerged during the last global post-glacial eustatic sea-level rise (Siddall et al.,
583 2003). During this transgression, the glacifluvial valley must have become an estuary, a similar
584 evolution to lakes Lanalhue and Lleu Lleu ~500 km further north (Fig. 1) (Stefer et al., 2010).
585 The oldest recovered sediment in core Pos04 (around tsunami deposit cN, reflector R6) is
586 lacustrine, indicating that the barrier, which makes Lake Cucao a coastal lake, rather than an
587 estuary, has been in place earlier than 4300 yrs ago.

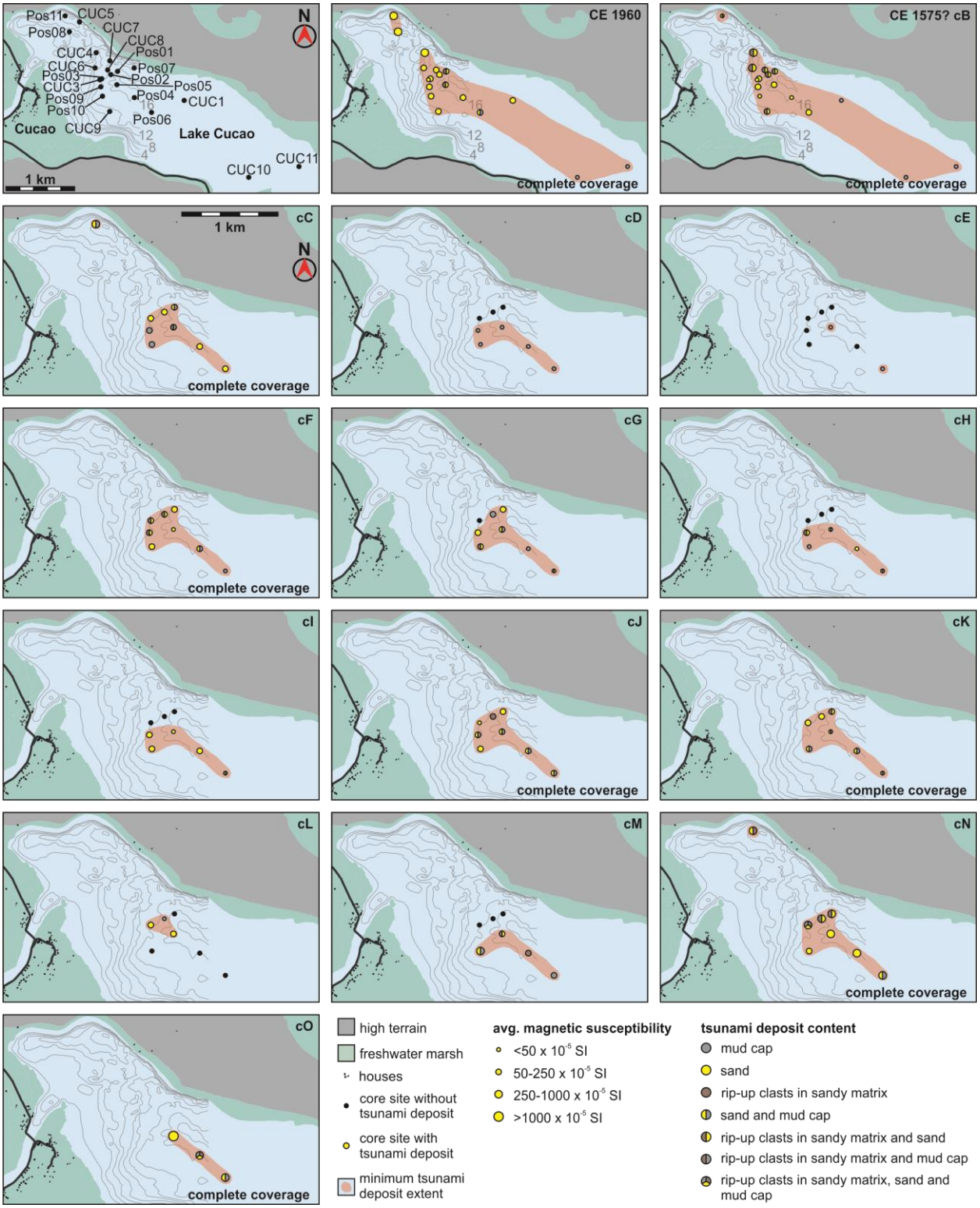

Figure 9: Event map of all tsunami deposit cA, i.e. CE 1960, to cO. The dots refer to core sites that contain the stratigraphic interval in which the tsunami deposit is located. Black dots mean the tsunami deposit was not detected. The size of the dot is a function of the average magnetic susceptibility over the entire tsunami deposit. The colour of the dot is a function of the sedimentary content of the tsunami deposit. The red polygon depicts the lateral extent of the tsunami deposit.

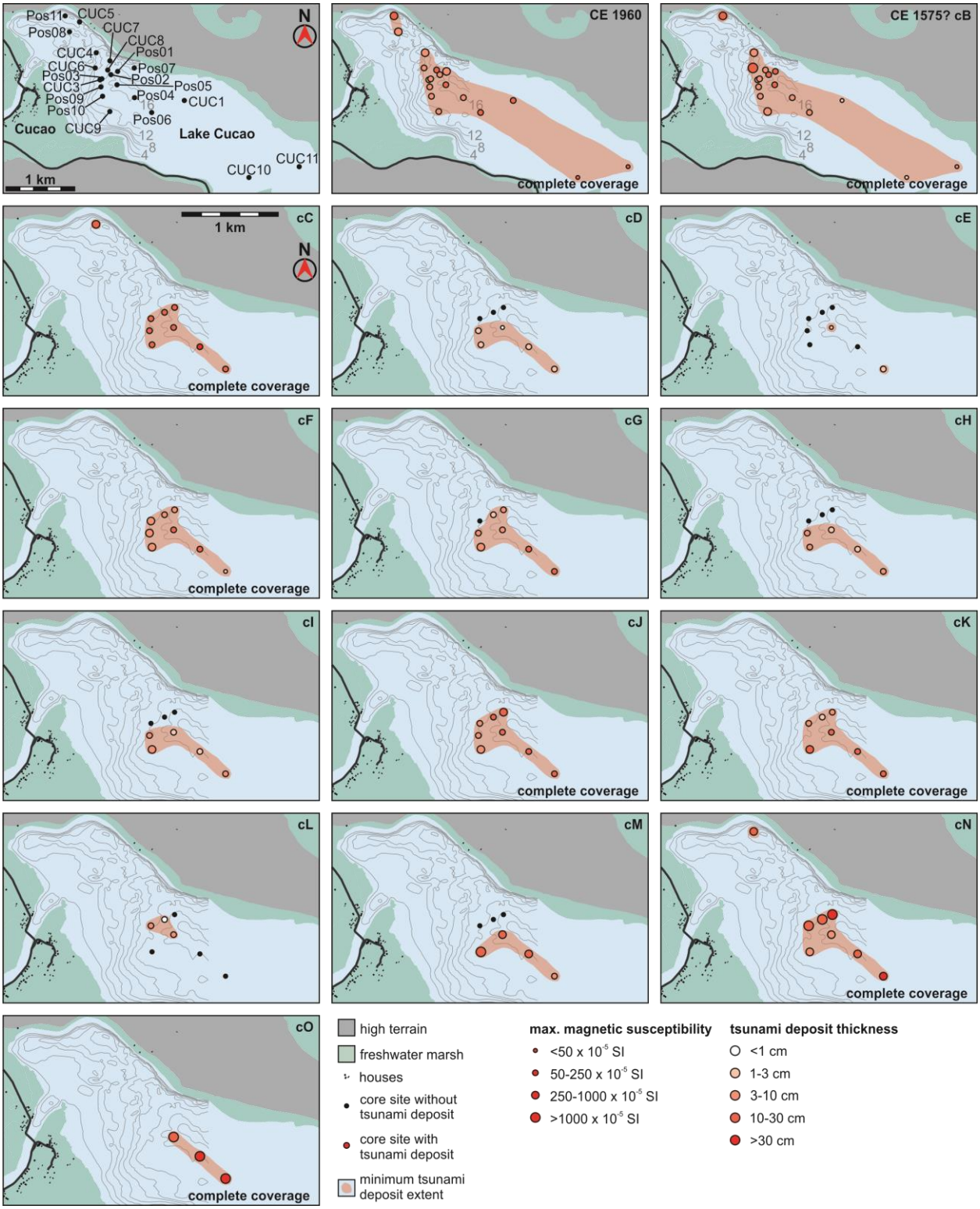

Figure 10: Event map of all tsunami deposit cA, i.e. CE 1960, to cO. The dots refer to core sites that contain the stratigraphic interval in which the tsunami deposit is located. Black dots mean the tsunami deposit was not detected. The size of the dot is a function of the maximum magnetic susceptibility of the tsunami deposit. The colour of the dot is a function of the tsunami deposit thickness in the core (darker red means thicker tsunami deposit). The red polygon depicts the lateral extent of the tsunami deposit.

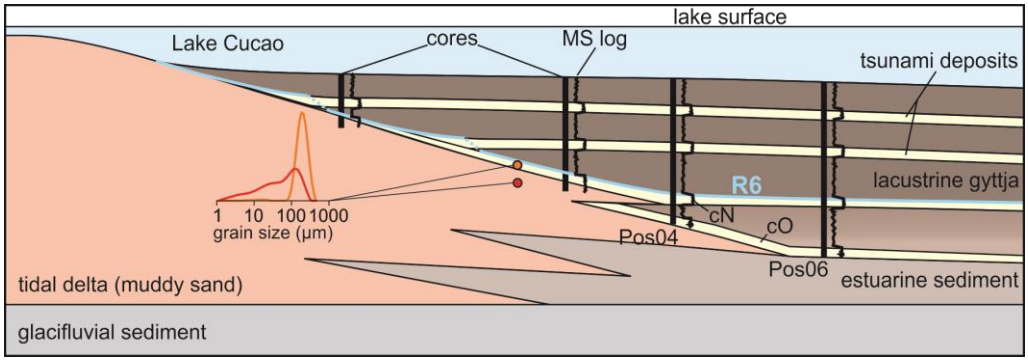

Figure 11: Conceptual stratigraphic model of Lake Cucao's sedimentary infill that summarizes the sedimentologic evidence available in the literature and in the results of this study. This model also explains the corrected age of tsunami deposit cO.

Most likely aeolian sediments silled off the estuary and created the barrier and therewith the enclosed lake basin. The timing of the sill formation is unclear, however, one plausible hypothesis is that the expanding westerlies between 8.5 and 5.5 ka (Lamy et al., 2010) may have enabled aeolian processes to create the sill. Aeolian processes are still prevailing in the coastal area west of Lake Cucao evidenced by an active dune belt.

Currently, Lake Cucao lies in the intertidal zone (Kempf et al., 2015; Villalobos et al., 2003), with saline water flowing into the lake from the Pacific during high tide. This process has been active at least sporadically since 4300 cal. yrs BP, evidenced by the convergent internal reflectors in the entire sediment sequence of U2 near the tidal channel. The same process has built up a tidal delta in Lake Cucao around the outlet. The conceptual stratigraphic model includes foresets of the tidal delta interfingering with lake basin and estuarine sediments (Fig. 11). One of these foresets may explain the muddy sand with the same characteristics as the exposed tidal delta sediments at the base of cores Pos02, Pos03 and Pos11. Clastic layer cN, interpreted as a tsunami deposit, is in direct contact to the muddy sand in all cores of the western part of the basin, except at Pos06. It appears that the formation of cN disrupted the deposition of muddy sand at the mentioned core locations. Clastic layer cN is thicker and coarser than all other clastic layers in most core locations. Additionally, the deposit correlates chronologically to deposit hN, which is among the thicker and coarser tsunami deposits from the nearby Lake Huelde paleotsunami record (Kempf et al., 2017).

The overall extreme character relative to other tsunami deposits in the respective records of cN and hN may point towards an unusually strong tsunami. The end of foreset sedimentation after deposition of cN could be due to a large amount of either co-seismic uplift or subsidence during this event.

In the uplift scenario the lake system may stop interacting with the Pacific Ocean altogether. Tidal inflows into the lake would not occur and the processes, which form topsets and foresets on the tidal delta, would stop. Large amounts of co-seismic uplift can occur on the Chilean coast, e.g. in CE 1960 on Isla Guafo (Sievers et al., 1963). However, the geometry of the crust on and off Chiloé Island probably needs splay fault slip to generate such an uplift and an outstanding tsunami, as neither CE 1960, 1837 nor 1575 created large co-seismic uplift there (Cisternas et al., 2017; Garrett et al., 2015; Plafker and Savage, 1970; Sievers et al., 1963).

The subsidence scenario seems more plausible, because of the example given by co-seismic subsidence around Cucao (~1 m) during the CE 1960 earthquake (Plafker and Savage, 1970). The subsidence would create accommodation, which would favour aggradation at the cost of progradation of the delta. During aggradation on the delta, the lake basin would accumulate organic-rich mud. Once aggradation used up the newly available accommodation, the lake system would switch back to progradation and begin forming the next interfingering foreset. In both examples, the presence of the tidal delta would be less dominant in the basinal sediments.

6 Conclusions

Based on sub-bottom profiles and numerous sediment cores, we add a new, long and continuous paleotsunami record in the rupture zone of the CE 1960 Great Chile Earthquake. We present following conclusions:

i) Sub-bottom profiles are crucial to understand the dynamic sedimentary system of coastal lakes and to help in selecting the most appropriate coring locations for paleotsunami research. Moreover, sub-bottom profiles may reveal sedimentary structures which can allow quantification of flow speed and depth, e.g. antidunes (Fig. 2).

ii) Dynamic coastal lakes with daily tidal inflow can be used for extracting long paleotsunami records. For the last 4300 yrs, Lake Cucao presents 15 tsunami deposits of mostly moderate to high confidence on the interpretation. This confidence level was based on physical sedimentary characteristics and contextual characteristics (Tab. 2), such as maximum magnetic susceptibility, traceability (Figs. 9 and 10), correlation to acoustic reflectors on the sub-bottom profiles (Fig. 6), the presence or lack of mud rip-up clasts (Figs. 5 and 9), and age correlation with regional paleotsunami (Fig. 8). At least 10 tsunami deposits correlate to paleotsunami deposits found in nearby Lake Huelde.

iii) The most complete tsunami record was found in core Pos05, 1.3 km from the lake outlet (tidal inlet) and a total 2.6 km from the present-day coastline. This relatively far inland location for regular tsunami deposition is facilitated by the river channel. There is evidence for tidal currents throughout the entire record, and thus persistent river connection, which allowed for continuous recording of tsunamis, despite co-, post- and inter-seismic relative sea level change in the late Holocene. However, such tidal currents can affect sediment dynamics, leading to variable depositional rates in space and time, adding complexity for reliable mapping and dating of tsunami deposits.

iv) This study underlines the many challenges and extraordinary advantages associated to paleotsunami research on coastal lakes and demonstrates how indispensable geophysical mapping and numerous coring sites are in understanding the depositional environment of dynamic coastal lakes for extracting high-quality, long and continuous paleotsunami records.

Acknowledgments

PK acknowledges financial support by the Special Research Fund of Ghent University (BOF), JM from the Chilean Fondecyt projects nr. 1150346 and 1150321, MVD from the Research Foundation Flanders (FWO travel grant K201512N), RU from CONICYT/FONDAP/15130015. We thank Koen De Rycker, Willem Vandoorne and Gauvain Wiemer for fieldwork support, Dr.

677 Claire Schepens and Dr. Eric Achten for CT-scanner support. IHS Markit is acknowledged for
678 providing the Kingdom seismic interpretation software within their educational grant program.

679 **References**

680 Allen, J.R.L., 1984. Sedimentary Structures: Their Character and Physical Basis. Elsevier,
681 Amsterdam.

682 Amante, C., Eakins, B.W., 2009. ETOPO1 1 Arc-Minute Global Relief Model: Procedures, Data
683 Sources and Analysis. NOAA Technical Memorandom NESDIS NGDC-24. National
684 Geophysical Data Center, NOAA. doi:10.7289/V5C8276M

685 Atwater, B.F., Cisternas, M., Yulianto, E., Prendergast, A.L., Jankaew, K., Eipert, A.A.,
686 Ignatius, W., Fernando, S., Tejakusuma, I., 2013. The 1960 tsunami on beach-ridge plains
687 near Maullín, Chile: Landward descent, renewed breaches, aggraded fans, multiple
688 predecessors. Andean Geology 40, 393–418. doi:10.5027/andgeoV40n3-a01

689 Blaauw, M., Christen, J.A., 2011. Flexible Paleoclimate Age-Depth Models Using an
690 Autoregressive Gamma Process. Bayesian Analysis 6, 457–474. doi:10.1214/11-BA618

691 Carling, P., Burr, D., Brennand, T.A., 2009. A review of open-channel megaflood depositional
692 landforms on Earth and Mars A review of open-channel megaflood depositional landforms
693 on Earth and Mars, in: Burr, D.M., Carling, P.A., Baker, V.R. (Eds.), Megaflooding on
694 Earth and Mars. pp. 33–49. doi:10.1017/CBO9780511635632.003

695 Chagué-Goff, C., Schneider, J.-L., Goff, J.R., Dominey-Howes, D., Strotz, L., 2011. Expanding
696 the proxy toolkit to help identify past events — Lessons from the 2004 Indian Ocean
697 Tsunami and the 2009 South Pacific Tsunami. Earth-Science Reviews 107, 107–122.
698 doi:10.1016/j.earscirev.2011.03.007

699 Chagué-Goff, C., Szczuciński, W., Shinozaki, T., 2017. Applications of geochemistry in tsunami
700 research: A review. Earth-Science Reviews 165, 203–244.
701 doi:https://doi.org/10.1016/j.earscirev.2016.12.003

702 Cisternas, M., Atwater, B.F., Torrejón, F., Sawai, Y., Machuca, G., Lagos, M., Eipert, A.,
703 Youlton, C., Salgado, I., Kamataki, T., Shishikura, M., Rajendran, C.P., Malik, J.K., Rizal,
704 Y., Husni, M., 2005. Predecessors of the giant 1960 Chile earthquake. Nature 437, 404–
705 407. doi:10.1038/nature03943

706 Cisternas, M., Garrett, E., Wesson, R., Dura, T., Ely, L.L., 2017. Unusual geologic evidence of
707 coeval seismic shaking and tsunamis shows variability in earthquake size and recurrence in
708 the area of the giant 1960 Chile earthquake. Marine Geology 385, 101–113.
709 doi:10.1016/j.margeo.2016.12.007

710 Dura, T., Cisternas, M., Horton, B.P., Ely, L.L., Nelson, A.R., Wesson, R.L., Pilarczyk, J.E.,
711 2015. Coastal evidence for Holocene subduction-zone earthquakes and tsunamis in central
712 Chile. Quaternary Science Reviews 113, 93–111. doi:10.1016/j.quascirev.2014.10.015

713 Dura, T., Engelhart, S.E., Vacchi, M., Horton, B.P., Kopp, R.E., Peltier, W.R., Bradley, S., 2016.
714 The Role of Holocene Relative Sea-Level Change in Preserving Records of Subduction
715 Zone Earthquakes. Current Climate Change Reports 2, 86–100. doi:10.1007/s40641-016-

716 0041-y

717 Ely, L.L., Cisternas, M., Wesson, R.L., Dura, T., 2014. Five centuries of tsunamis and land-level
718 changes in the overlapping rupture area of the 1960 and 2010 Chilean earthquakes. Geology
719 42, 995–998. doi:10.1130/G35830.1

720 Fedorov, A. V, Brierley, C.M., Emanuel, K., 2010. Tropical cyclones and permanent El Niño in
721 the early Pliocene epoch. Nature 463, 1066–1070. doi:10.1038/nature08831

722 Fritz, H.M., Phillips, D.A., Okayasu, A., Shimozono, T., Liu, H., Mohammed, F., Skanavis, V.,
723 Synolakis, C.E., Takahashi, T., 2012. The 2011 Japan tsunami current velocity
724 measurements from survivor videos at Kesennuma Bay using LiDAR. Geophysical
725 Research Letters 39, 6. doi:10.1029/2011GL050686

726 Garrett, E., Shennan, I., Woodroffe, S.A.A., Cisternas, M., Hocking, E.P.P., Gulliver, P., 2015.
727 Reconstructing paleoseismic deformation, 2: 1000 years of great earthquakes at Chucalén,
728 south central Chile. Quaternary Science Reviews 113, 112–122.
729 doi:10.1016/j.quascirev.2014.10.010

730 Glasser, N.F., Jansson, K.N., Harrison, S., Kleman, J., 2008. The glacial geomorphology and
731 Pleistocene history of South America between 38°S and 56°S. Quaternary Science Reviews
732 27, 365–390. doi:10.1016/j.quascirev.2007.11.011

733 Goto, K., Hashimoto, K., Sugawara, D., Yanagisawa, H., Abe, T., 2014. Spatial thickness
734 variability of the 2011 Tohoku-oki tsunami deposits along the coastline of Sendai Bay.
735 Marine Geology 358, 38–48. doi:10.1016/j.margeo.2013.12.015

736 Heiri, O., Lotter, A.F., Lemcke, G., 2001. Loss on ignition as a method for estimating organic
737 and carbonate content in sediments : reproducibility and comparability of results. Journal of
738 Paleolimnology 25, 101–110. doi:10.1023/A:1008119611481

739 Hogg, A.G., Hua, Q., Blackwell, P.G., Niu, M., Buck, C.E., Guilderson, T.P., Heaton, T.J.,
740 Palmer, J.G., Reimer, P.J., Reimer, R.W., Turney, C.S.M., Zimmerman, S.R.H., 2013.
741 SHCal13 Southern Hemisphere Calibration, 0–50,000 Years cal BP. Radiocarbon 55, 1889–
742 1903. doi:10.2458/azu_js_rc.55.16783

743 Kelsey, H.M., Engelhart, S.E., Pilarczyk, J.E., Horton, B.P., Rubin, C.M., Daryono, M.R.,
744 Ismail, N., Hawkes, A.D., Bernhardt, C.E., Cahill, N., 2015. Accommodation space,
745 relative sea level, and the archiving of paleo-earthquakes along subduction zones. Geology
746 43, 675–678. doi:10.1130/G36706.1

747 Kelsey, H.M., Nelson, A.R., Hemphill-Haley, E., Witter, R.C., 2005. Tsunami history of an
748 Oregon coastal lake reveals a 4600 yr record of great earthquakes on the Cascadia
749 subduction zone. Geological Society of America Bulletin 117, 1009–1032.
750 doi:10.1130/B25452.1

751 Kempf, P., 2016. Tsunamis in south central Chile: evidence from coastal lakes. Ghent
752 University.

753 Kempf, P., Moernaut, J., Batist, M. De, 2018. Bimodal Recurrence Pattern of Tsunamis in

754 South-Central Chile: A Statistical Exploration of Paleotsunami Data. Seismological
755 Research Letters 90, 194–202. doi:10.1785/0220180204

756 Kempf, P., Moernaut, J., Van Daele, M., Vandoorne, W., Pino, M., Urrutia, R., De Batist, M.,
757 2017. Coastal lake sediments reveal 5500 years of tsunami history in south central Chile.
758 Quaternary Science Reviews 161, 99–116.
759 doi:http://doi.org/10.1016/j.quascirev.2017.02.018

760 Kempf, P., Moernaut, J., Van Daele, M., Vermassen, F., Vandoorne, W., Pino, M., Urrutia, R.,
761 Schmidt, S., Garrett, E., De Batist, M., 2015. The sedimentary record of the 1960 tsunami
762 in two coastal lakes on Isla de Chiloé, south central Chile. Sedimentary Geology 328, 73–
763 86. doi:10.1016/j.sedgeo.2015.08.004

764 Kennedy, J., 1963. The mechanics of dunes and antidunes in erodible-bed channels. Journal of
765 Fluid Mechanics 16, 521–544. doi:10.1017/S0022112063000975

766 Kortekaas, S., Dawson, A.G., 2007. Distinguishing tsunami and storm deposits: An example
767 from Martinhal, SW Portugal. Sedimentary Geology 200, 208–221.
768 doi:https://doi.org/10.1016/j.sedgeo.2007.01.004

769 Lamy, F., Kilian, R., Arz, H.W., Francois, J.-P., Kaiser, J., Prange, M., Steinke, T., 2010.
770 Holocene changes in the position and intensity of the southern westerly wind belt. Nature
771 Geosci 3, 695–699.

772 Lee, Sang Hoon, Jung, W.-Y., Bahk, J.J., Gardner, J.M., Kim, J.K., Lee, Su Hwan, 2013.
773 Depositional features of co-genetic turbidite–debrite beds and possible mechanisms for their
774 formation in distal lobated bodies beyond the base-of-slope, Ulleung Basin, East Sea (Japan
775 Sea). Marine Geology 346, 124–140. doi:10.1016/j.margeo.2013.09.001

776 Lomnitz, C., 2004. Major Earthquakes of Chile: A Historical Survey, 1535-1960. Seismological
777 Research Letters 75, 368–378. doi:10.1785/gssrl.75.3.368

778 Lomnitz, C., 1970. Major Earthquakes and Tsunamis in Chile during the period 1535 to 1955.
779 Geologische Rundschau 59, 938–960.

780 Moernaut, J., Van Daele, M., Fontijn, K., Heirman, K., Kempf, P., Pino, M., Valdebenito, G.,
781 Urrutia, R., Strasser, M., De Batist, M., 2018. Larger earthquakes recur more periodically:
782 New insights in the megathrust earthquake cycle from lacustrine turbidite records in south-
783 central Chile. Earth and Planetary Science Letters 481, 9–19.
784 doi:https://doi.org/10.1016/j.epsl.2017.10.016

785 Moernaut, J., Van Daele, M., Heirman, K., Fontijn, K., Strasser, M., Pino, M., Urrutia, R., De
786 Batist, M., 2014. Lacustrine turbidites as a tool for quantitative earthquake reconstruction:
787 New evidence for a variable rupture mode in south central Chile. Journal of Geophysical
788 Research: Solid Earth 119, 1607–1633. doi:10.1002/2013JB010738

789 Moreno, M.S., Bolte, J., Klotz, J., Melnick, D., 2009. Impact of megathrust geometry on
790 inversion of coseismic slip from geodetic data: Application to the 1960 Chile earthquake.
791 Geophysical Research Letters 36, L16310. doi:10.1029/2009GL039276

792 Nentwig, V., Bahlburg, H., Górecka, E., Huber, B., Bellanova, P., Witkowski, A., Encinas, A.,
793 2018. Multiproxy analysis of tsunami deposits—The Tirúa example, central Chile.
794 Geosphere 14, 1067–1086. doi:10.1130/GES01528.1

795 Nentwig, V., Tsukamoto, S., Frechen, M., Bahlburg, H., 2015. Reconstructing the tsunami
796 record in Tirúa, Central Chile beyond the historical record with quartz-based SAR-OSL.
797 Quaternary Geochronology 30, 299–305.
798 doi:http://dx.doi.org/10.1016/j.quageo.2015.05.020

799 Peters, R., Jaffe, B., Gelfenbaum, G., 2007. Distribution and sedimentary characteristics of
800 tsunami deposits along the Cascadia margin of western North America. Sedimentary
801 Geology 200, 372–386. doi:10.1016/j.sedgeo.2007.01.015

802 Phantuwongraj, S., Choowong, M., Nanayama, F., Hisada, K.-I., Charusiri, P., Chutakositkanon,
803 V., Pailoplee, S., Chabangbon, A., 2013. Coastal geomorphic conditions and styles of storm
804 surge washover deposits from Southern Thailand. Geomorphology 192, 43–58.
805 doi:10.1016/j.geomorph.2013.03.016

806 Plafker, G., Savage, J.C., 1970. Mechanism of the Chilean Earthquakes of May 21 and 22 , 1960.
807 Geological Society of America Bulletin 81, 1001–1030. doi:10.1130/0016-7606(1970)81

808 Reinhardt, E.G., Nairn, R.B., Lopez, G., 2010. Recovery estimates for the Río Cruces after the
809 May 1960 Chilean earthquake. Marine Geology 269, 18–33.
810 doi:10.1016/j.margeo.2009.12.003

811 Siddall, M., Rohling, E.J., Almogi-Labin, A., Hemleben, C., Meischner, D., Schmelzer, I.,
812 Smeed, D.A., 2003. Sea-level fluctuations during the last glacial cycle. Nature 423, 853–
813 858.

814 Sievers, H., Villegas, G.C., Barros, G., 1963. The seismic sea wave of 22 May 1960 along the
815 Chilean coast. Bulletin of the Seismological Society of America 53, 1125–1190.

816 Stefer, S., Moernaut, J., Melnick, D., Echtler, H.P., Arz, H.W., Lamy, F., De Batist, M., Oncken,
817 O., Haug, G.H., 2010. Forearc uplift rates deduced from sediment cores of two coastal lakes
818 in south-central Chile. Tectonophysics 495, 129–143.
819 doi:http://dx.doi.org/10.1016/j.tecto.2009.05.006

820 Valdovinos, C., Pedreros, P., 2007. Geographic variations in shell growth rates of the mussel
821 Diplodon chilensis from temperate lakes of Chile: Implications for biodiversity
822 conservation. Limnologica 37, 63–75. doi:https://doi.org/10.1016/j.limno.2006.08.007

823 Van Daele, M., Araya-Cornejo, C., Pille, T., Vanneste, K., Moernaut, J., Schmidt, S., Kempf, P.,
824 Meyer, I., Cisternas, M., 2019. Distinguishing intraplate from megathrust earthquakes using
825 lacustrine turbidites. Geology 47, 127–130.

826 Van Daele, M., Cnudde, V., Duyck, P., Pino, M., Urrutia, R., De Batist, M., 2014.
827 Multidirectional, synchronously-triggered seismo-turbidites and debrites revealed by X-ray
828 computed tomography (CT). Sedimentology 61, 861–880. doi:10.1111/sed.12070

829 Villalobos, L., Parra, O., Grandjean, M., Jaque, E., Woelfl, S., Campos, H., 2003. A study of the

river basins and limnology of five humic lakes on Chiloé Island. Revista chilena de historia natural 76. doi:10.4067/S0716-078X2003000400003

Wesson, R.L., Melnick, D., Cisternas, M., Moreno, M., Ely, L.L., 2015. Vertical deformation through a complete seismic cycle at Isla Santa Maria, Chile. Nature Geoscience 8, 547–551.